

# Electrical active power optimization of the SEIG-WTS based on perturb and observe method

Mario G. Borja Borja<sup>1</sup>, Sergio Lescano<sup>2</sup>, Sally Torres Alvarado<sup>3</sup>, Ubaldo Yancachajlla Tito<sup>4</sup>, Jaime Luyo<sup>1</sup>

<sup>1</sup>System Control, Automatic and Industrial Robotics Research Laboratory, Department of Mechanical Engineering, National University of Engineering, Lima, Peru

<sup>2</sup>AMAROB Technologies, Besancon, France

<sup>3</sup>Dynamic of Systems and Natural Language Processing Research Laboratory, Department of Systems Engineering, National University of Callao, Lima, Peru

<sup>4</sup>Wind Energy Research Laboratory, Department of Engineering Sciences, National University of Juliaca, Juliaca, Peru

---

## Article Info

### Article history:

Received Jun 10, 2023

Revised Jan 17, 2024

Accepted Sep 28, 2024

---

### Keywords:

Maximum power point tracking control

Perturb and observe approach

Self-excited induction generator

Squirrel cage induction generator

Wind energy conversion

Wind turbine

---

## ABSTRACT

This paper proposes an electrical active power optimization for self-excited induction generator-wind turbine system (SEIG-WTS) using a perturb and observe (P&O)-based maximum power point tracking. The main advantage is the optimization of the SEIG active power of SEIG-WTS and the simply practical implementation with rotor speed sensor, current sensor and three phase inverter. The active power optimization of SEIG-WTS is achieved by perturbing angular magnetic field speed with stator reference voltage. To test the effectiveness of the proposal, numeric simulations were carried out under very challenging conditions with wind speed profile in steps and actual wind speed profile. The proposal reaches the maximum power in 7 seconds for hardest condition when the system works at high rotor speed. The proposal is useful for the development of maximum power point tracking control (MPPT) controllers due to its simplicity in implementation.

*This is an open access article under the [CC BY-SA](#) license.*



---

## Corresponding Author:

Mario G. Borja Borja

System Control, Automatic and Industrial Robotics Research Laboratory  
Department of Mechanical Engineering, National University of Engineering  
Lima, Peru

Email: [mborjab@uni.edu.pe](mailto:mborjab@uni.edu.pe)

---

## 1. INTRODUCTION

Wind energy conversion systems (WECS) with self-excited induction generator (SEIG) are widely used in stand-alone applications because SEIG is robust, low-maintenance, and low-cost. Unlike other generators such as permanent-magnet and doubly-feed that are easy to control but they are high cost. The SEIG with excitation capacitors has been widely documented as in [1] where a dynamical model of induction generator used in wind energy systems is presented, in [2] the influence of iron losses on selecting the minimum capacitance excitation is shown, the influence of residual magnetism in the SEIG are shown in [3], and control with STATCOM is shown in [4], [5].

Another option is to use the self-excited induction generator-wind turbine system (SEIG-WTS) is controlling the dc-link voltage or the maximum power point and produced electrical energy charges the battery bank. Among the dc-link voltage controllers, the direct field-oriented control [6]-[8] and the

indirect field-oriented control [9]-[11] for SEIG are widely employed. Due to the continuous wind speed changes, to optimize the power extraction from a WECS requires the development of maximum power point tracking (MPPT) control algorithms. Some of those MPPT algorithms discussed in the work [12] are applied. These algorithms are classified into: i) indirect power control (IPC), ii) direct power control (DPC), iii) hybrid MPPT algorithms, and iv) smart MPPT algorithms. An incremental conductance (INC) MPPT algorithm, using the perturb and observe (P&O) method, where the perturbed variable is the DC-link voltage and the observed variable is the DC-link power is presented in [13], it controls the DC-link voltage using an insulated gate bipolar transistor that allows the voltage to be switched in an RC circuit. The power signal feedback (PSF) MPPT algorithms presented in [14]-[17], use indirect methods to determine the maximum power point of the turbine, either through experimental data tables, speed observers or speed sensors and various methods of control of the angular rotor speed of the generator are used.

Despite the latest advances of MPPT for SEIG-WTS presented in [18]-[28] are PSF-type MPPT algorithms, focusing on extracting the maximum power from the wind turbine, controlling the angular rotor speed of the generator at the speed that the wind turbine captures maximum power, using previously stored experimental data. However, the maximum power point of the SEIG-wind turbine system is not always the maximum power point of the wind turbine as shown in [29]. Based on these findings, an global MPPT algorithm for electrical active power optimization of the SEIG-WTS is presented in this paper. The key benefits of the presented electrical active power optimization of the SEIG-WTS are the maximization of the useful electrical power, low cost of the SEIG and simple implementation of the MPPT algorithm. Another advantage of the proposal is that common self-excited induction motors can be used as generator. The idea is based on power optimization using the SEIG-WTS global power curve, which is distinct from the separate SEIG and wind turbine power curve. Unlike other approaches optimize the mechanical wind turbine power.

The method is explained in section 2, the complete MPPT algorithm is presented in section 2.2. In section 3, detailed test results are presented. Finally, in section 4, the conclusions and future recommendation are given.

## 2. METHOD

### 2.1. Self-excited in-duction generator-wind turbine system mathematical model

The SEIG-WTS dynamic mathematical model in stationary reference frame of the stator ( $a - b$ ) in (1) is obtained by joining the two-phase model of the SEIG with one pair of poles of [11] in stationary reference frame (ab axis) and the wind turbine model of [30]. In the model, the wind turbine torque  $T_a$  is applied to the generator rotor through a gearbox with the transmission ratio  $i$ .

$$\begin{aligned}
 \dot{i}_a &= -\gamma i_a + \alpha\beta\psi_a + \beta\omega\psi_b + \sigma^{-1}u_a, \\
 \dot{i}_b &= -\gamma i_b + \alpha\beta\psi_b - \beta\omega\psi_a + \sigma^{-1}u_b, \\
 \dot{\psi}_a &= -\alpha\psi_a - \omega\psi_b + \alpha L_m i_a, \\
 \dot{\psi}_b &= -\alpha\psi_b + \omega\psi_a + \alpha L_m i_b, \\
 P_s &= -\frac{3}{2}(u_a i_a + u_b i_b), \\
 \dot{\omega} &= (\frac{1}{J})(T - T_c), \quad T = \mu(\psi_a i_b - \psi_b i_a), \\
 T_c &= T_a i, \quad T_a = \frac{1}{2\omega_r} \rho A V_r^3 C_p, \\
 C_p &= C_1 \left( \frac{C_2}{\lambda_i} - C_3 - C_4 \right) e^{-\frac{C_5}{\lambda_i}} + C_6 \lambda, \quad \lambda = \frac{\omega_r R}{V_r}, \\
 \frac{1}{\lambda_i} &= \frac{1}{\lambda + 0.08\beta} - \frac{0.035}{\beta^3 + 1}, \\
 P_a &= P_w C_p \quad P_w = 0.5 \rho A V_r^3,
 \end{aligned} \tag{1}$$

where  $\omega$  is the angular rotor speed,  $\mathbf{i} = (i_a, i_b)^T$  is the stator current vector,  $\mathbf{u} = (u_a, u_b)^T$  is the stator voltages vector,  $\Psi = (\Psi_a, \Psi_b)^T$  is the rotor flux vector and  $P_s$  is the SEIG active power. In the wind turbine model,  $A$  is swept area,  $R$  is the blade length,  $C_p$  is power coefficient,  $\lambda$  is the tip speed ratio,  $\beta$  is the blade pitch angle,

$V_r$  is the wind speed in the rotor plane,  $\rho$  is the air density, and  $C_1, C_2, C_3, C_4, C_5$ , and  $C_6$  are the wind turbine constant coefficients. The mechanical and electrical parameters of the generator are calculated with:

$$\alpha = \frac{R_2}{L_2}, \quad \sigma = L_1(1 - \frac{L_{m2}}{L_1 L_2}), \quad \beta = \frac{L_m}{\sigma L_2}, \quad \gamma = \frac{R_1}{\sigma} + \alpha L_m \beta, \quad \mu = \frac{3L_m}{2L_2} \quad (2)$$

where  $L_m$  is the magnetization inductance,  $R_1, R_2, L_1$ , and  $L_2$  are the stator and rotor resistances and inductances respectively.

## 2.2. Maximum power point tracking control algorithm

The SEIG active power is controlled by the angular magnetic field speed generated by the reference voltage applied to the stator winding, and it is different for each value of rotor angular speed of the SEIG. On the other hand, the SEIG-WTS maximum power point is different from the wind turbine maximum power point. In the P&O optimization method, a system variable is perturbed that causes the observed variable to be incremented, this process is repeated until the observed variable begins to decrease, taking the last largest value as the maximum. In the SEIG-WTS, the power used by the final user is the SEIG active power, for which the MPPT algorithm is proposed using the SEIG active power as the observed variable and the angular magnetic field speed as the perturbed variable. The two-phase reference voltage applied to the stator of the SEIG is calculated with (3):

$$\begin{aligned} u_a &= u_n \cos(\omega_0 t), \\ u_b &= u_n \sin(\omega_0 t) \end{aligned} \quad (3)$$

where  $u_n$ ,  $\omega_0$ , and  $t$  are the voltage amplitude, stator magnetic field angular speed and time. And the SEIG active power is calculated with (4):

$$P_s = -\frac{3}{2}(u_a i_a + u_b i_b), \quad (4)$$

where  $u_a$  and  $u_b$  are the stator voltage components, and  $i_a$  and  $i_b$  are the stator current components.

The proposed MPPT algorithm, represented in the flowchart of Figure 1 uses the variables: angular rotor speed of the current measurement ( $\omega$ ); angular rotor speed from the previous measurement ( $\omega_a$ ); increment that the angular rotor speed must vary to recalculate the new value of the maximum power point ( $\Delta\omega$ ); increase in the angular magnetic field speed ( $\Delta\omega_0$ ); current angular magnetic field speed ( $\omega_0$ ); previous angular magnetic field speed ( $\omega_{0a}$ ); current active power ( $P_s$ ); previous active power ( $P_{sa}$ ); maximum active power ( $P_{max}$ ); component  $a$  of the stator reference voltage ( $u_a$ ); and component  $b$  of the stator reference voltage ( $u_b$ ).

When the operation of the proposed MPPT algorithm starts, the SEIG-WTS rotor rotates at a certain angular speed due to the effect of the wind at that instant, which is measured by the sensor, and if the change of rotor angular speed between the previous  $\omega_a$  and the current  $\omega$  measurement is greater than  $\Delta\omega$ , it starts the search process for the optimal value of  $\omega_0$  in which the system generates the maximum power. For this,  $P_s, P_{sa}, P_{max}$ , and  $\omega_{0a}$  are initialized with zero; the measured rotor speed value  $\omega$  is assigned to the magnetic field speed value  $\omega_0$  as the initial value; the value of  $\omega_0$  is decreased by  $\Delta\omega_0$ , with the new value of  $\omega_0$  the stator voltages values  $u_a$  and  $u_b$  are calculated; the new voltages values are applied to the stator through the three-phase bridge using pulse width modulation; the stator currents  $i_a$  and  $i_b$  are measured and the active power is calculated with (4). If the active power value  $P_s$  is greater than  $P_{max}$ , the new value of  $P_s$  is saved as the old value in  $P_{sa}$ , the value of  $P_s$  is saved as new value of  $P_{max}$ ,  $\omega_0$  is saved as the previous value  $\omega_{0a}$  and the value of  $\omega_0$  is again reduced by  $\Delta\omega$ . The operation is repeated until the new power value  $P_s$  is less than the value of  $P_{max}$ . This condition means that the active power  $P_s$  begins to decrease, then  $\omega_{0a}$  is resumed as the point of maximum power and is maintained until there is a change in angular rotor speed greater than  $\Delta\omega$ .

The control system hardware to implement the proposed MPPT is comprised by: rotor angular speed sensor (rotary encoder), two stator current sensors (hall effect sensors), three phase inverter and digital signal controller (DSC) as shown in the control system structure of the SEIG-WTS in the Figure 2. The MPPT software runs on the DSC, which reads the angular rotor speed from the angular speed sensor, assigns the initial value of the angular magnetic field speed, calculates the instantaneous value of the three phase voltages and generates the PWM to control the inverter to apply the reference voltage to the SEIG, then read the currents

of two phases and the current of the third phase is calculated, and with the calculated voltage value the active power of the SEIG is calculated, if it is not the maximum power it reduces the angular magnetic field speed and repeat the process until reaching the maximum power.

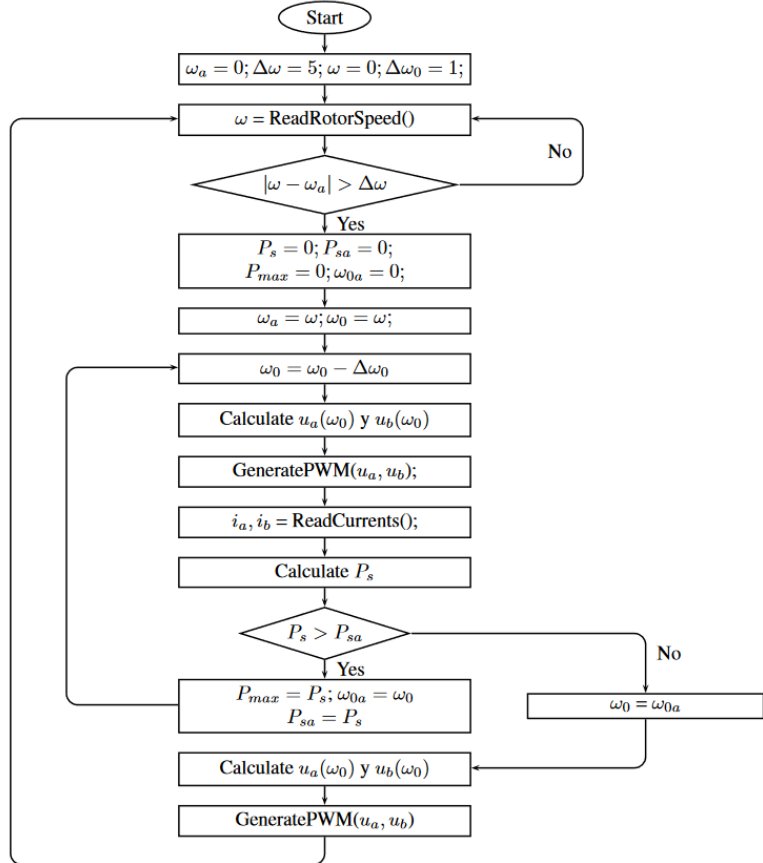


Figure 1. Proposed MPPT algorithm flowchart

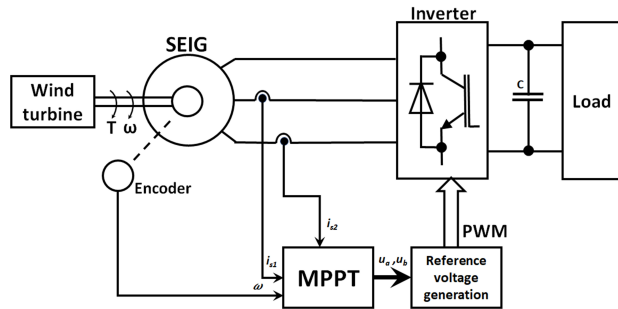


Figure 2. Control system structure of the SEIG-WTS with proposed MPPT

### 3. SIMULATION RESULTS AND DISCUSSION

The proposed MPPT algorithm is tested in a computational SEIG-WTS model using the mathematical model of (1), developed on Visual C++ applying the Euler numerical method to solve differential equations and the MPPT was implemented based on the algorithm of the Figure 1. The base test system is comprised by: three-phase SEIG and wind turbine. The SEIG-WTS parameters are presented in Table 1.

Table 1. SEIG-WTS parameters

Parameter	Value	Unit
Rated phase-voltage, rms	160	V
Rated phase-current, rms	5	A
Rated frequency	16	Hz
Number of poles	2	Poles
Stator resistance	5.3	$\Omega$
Rotor resistance	3.3	$\Omega$
Stator inductance	0.365	H
Rotor inductance	0.375	H
Magnetizing inductance	0.345	H
Rotor moment of inertia	0.0075	$kg.m^2$
Air density	0.9	$kg/m^3$
Swept area	10	$m^2$
Blade pitch angle	0	$^\circ$
Tip speed ratio	15	
Blade length	0.8	m
Transmission ratio	4	

The test results of the wind turbine computational model at wind speeds of 2, 4, 6, and 8 m/s are shown in Figure 3(a) the mechanical power and in Figure 3(b) the wind turbine torque. The mechanical power and rotor torque curves correspond to a wind turbine that have a maximum value for each wind speed value at a specific value of angular rotor speed. The tests of the WTS-SEIG system were carried out with three types of wind speed profiles: The first, with a constant wind speed profile; the second, applying a wind speed profile in steps and the last, with actual wind speed profile.

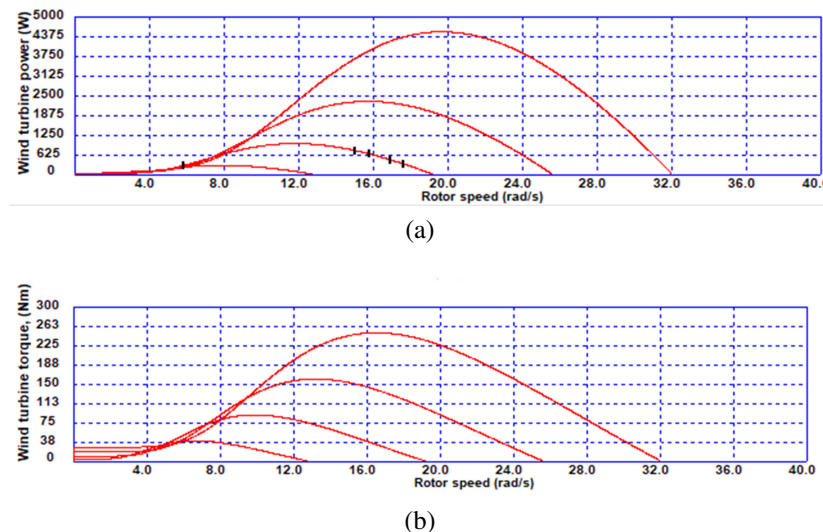


Figure 3. Wind turbine test results at 2, 4, 6, and 8 m/s wind speed; (a) wind turbine power and (b) wind turbine torque

The first test was carried out with a constant wind speed profile of 6 m/s as shown in Figure 4(a) for 1 s. The wind applied to the wind turbine generates a torque on the axis of the system that raises the rotor speed to approximately 130 rad/s in 0.3 s as shown in the Figure 4(b), then the MPPT algorithm starts the operation, calculating the field speed shown in Figure 4(b) and generates the stator reference voltage presented in the Figure 5(a), this reference voltage generates stator currents in the Figure 5(b) and the active power in Figure 6. The proposed MPPT algorithm reduces the field speed every 0.2 s, increasing the active power until reaching the maximum. As shown in Figure 4(b), the field speed is reduced by 0.4 s, 0.6 s, and 0.8 s by increasing the active power shown in Figure 6.

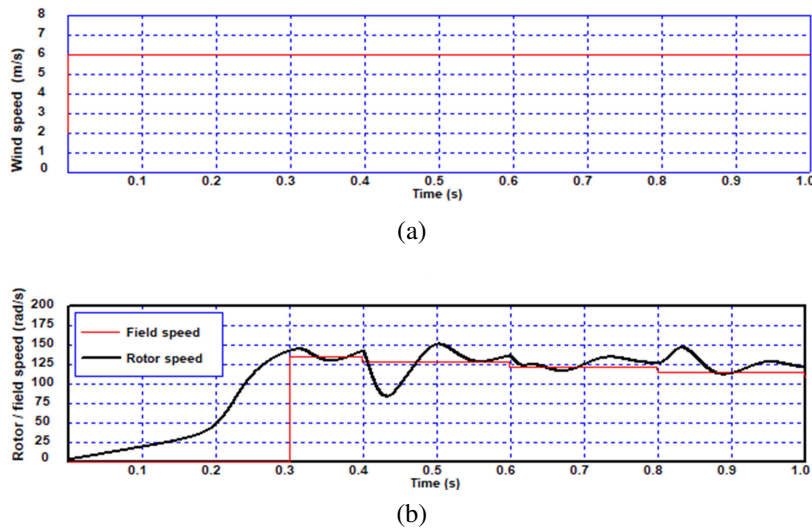


Figure 4. Wind turbine test results at 6 m/s wind speed; (a) wind speed and (b) rotor and field speed

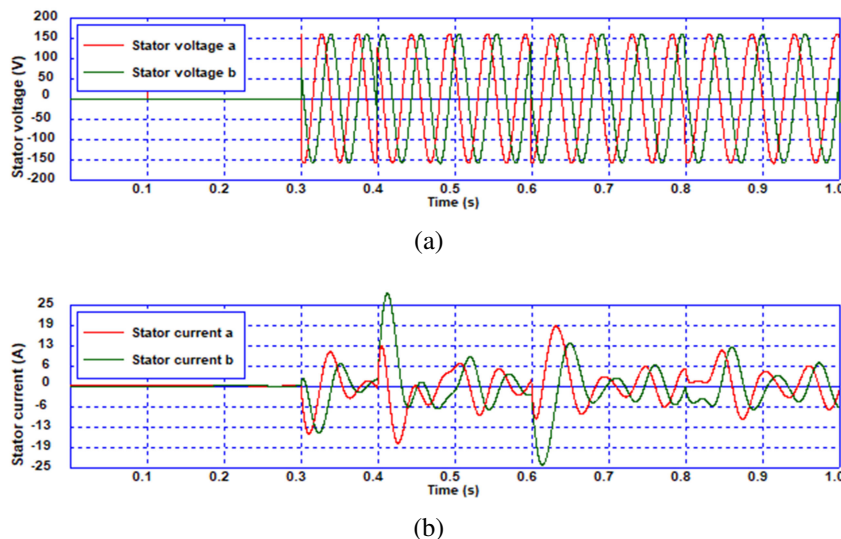


Figure 5. Wind turbine test results 6 m/s wind speed; (a) stator voltages and (b) stator currents

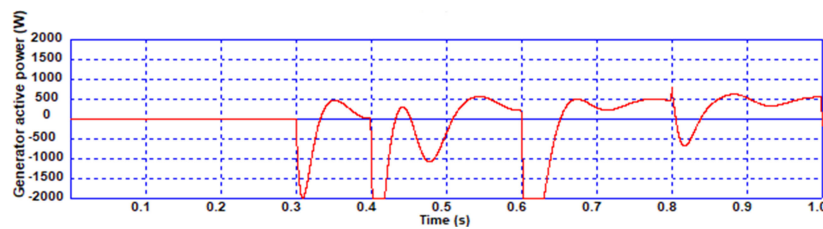


Figure 6. SEIG-WTS test result at 6 m/s wind speed

The second test was carried out with a wind speed profile in steps shown in Figure 7(a) with wind speeds of 4, 6, 8, 10, and 7 m/s. Figure 7(b) shows the torque generated by the wind turbine in the rotor of the system for each value of wind speed. This torque increases the rotor speed until the MPPT algorithm generates

the field speed shown in Figure 7(c) which is continuously reduced to reach the maximum power point as shown in Figure 7(d).

Figure 7(c) shows that at times 10, 20, 30, and 40 s, as the wind speed changes, the MPPT algorithm applies a field speed of 0 rad/s for 0.1 s, and the rotor speed of the system is increased by the effect of the wind turbine torque. Afterwards, the reduction of the field speed begins from an initial value close to the rotor speed until the point of maximum active power is reached and the rotor speed is reduced to the optimal value. Figure 7(d) shows the active power where it reaches the maximum value in the interval of 20 to 30 s at a wind speed of 8 m/s and the rotor speed is close to the nominal angular speed, for high and low wind speeds, the active power is lower. The maximum time to reach the maximum power point is 8 s, as can be seen in the range of 20 to 30 s.

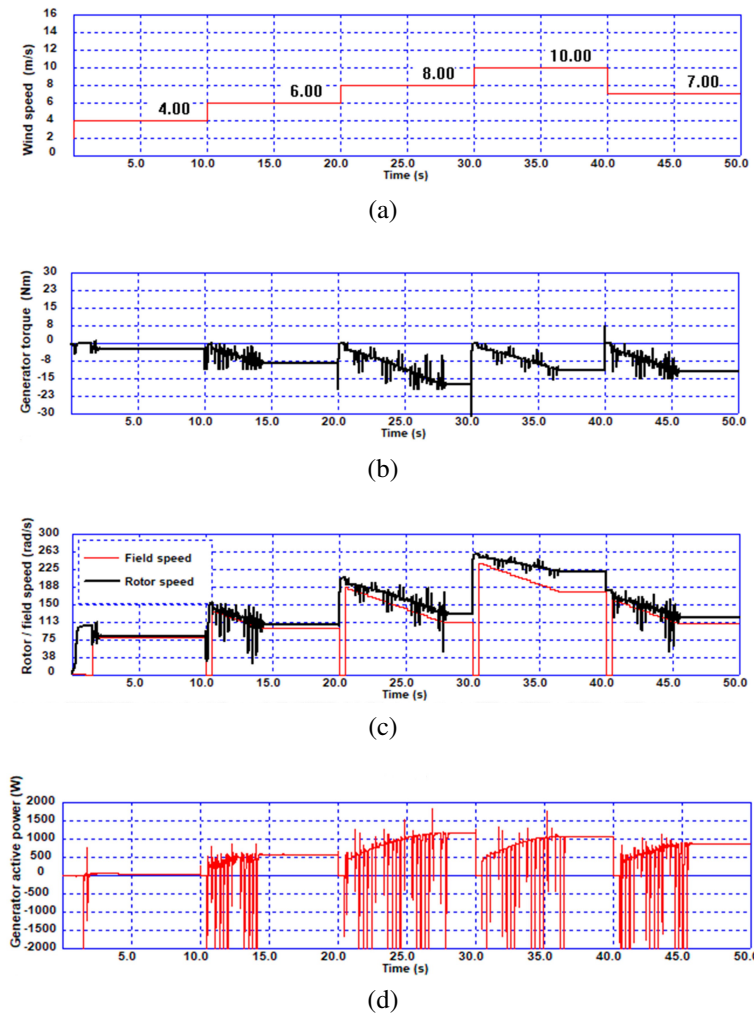


Figure 7. MPPT test results in the SEIG-WTS with a wind speed profile in steps; (a) wind speed profile, (b) generator torque, (c) rotor and magnetic field speed, and (d) generator active power

Finally, the proposed MPPT algorithm was tested with actual wind speed profile, which was measured from a wind farm [30] as shown in Figure 8 for 28,000 seconds. As shown in the Figure 8, the actual wind speed data is between 2.5 m/s to 17.5 m/s. The actual wind speed changes with an upward or downward trend as shown at the bottom of the Figure 8, where the 200-second data is presented starting from the 9,000th second of the total data set. The MPPT tests were performed for intervals of 10 and 50 seconds starting at the 15,000th second.

The proposed MPPT algorithm was tested with actual wind speed profile, where the wind speed changes continuously between 8.75 and 12.25 m/s for 10 seconds as shown in Figure 9(a). The results of

the MPPT operation test, which perturbs the magnetic angular field speed as shown in Figure 9(b), until reaching the maximum active power point as shown in Figure 9(c). The MPPT algorithm starts searching for the maximum power point when it detects a change in the rotor angular speed greater than  $\Delta\omega$ . First, release the rotor by applying a field speed zero value for 2 seconds so that the rotor reaches the maximum no-load speed, and then start with a field speed value close to the angular speed of the rotor and reduce by  $\Delta\omega_0$ , until reaching the maximum power point as presented in Figure 9(b). Rotor angular speed changes greater than  $\Delta\omega$  are approximately at times 0.9, 2.5 and 5.8 seconds as shown in Figure 9(b), where it is shown that when the angular velocity of the field changes, the angular velocity of the rotor begins a transient process as does the active power shown in Figure 9(c). The operation result of the proposed MPPT algorithm with the actual wind speed profile shown in Figure 9(a) is the generated active power curve shown in Figure 9(c) with an average of 0.75 kW.

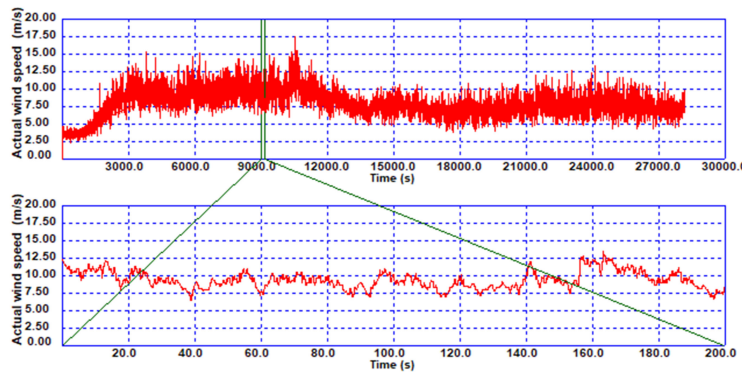


Figure 8. Actual wind profile used to test the proposed MPPT [30]

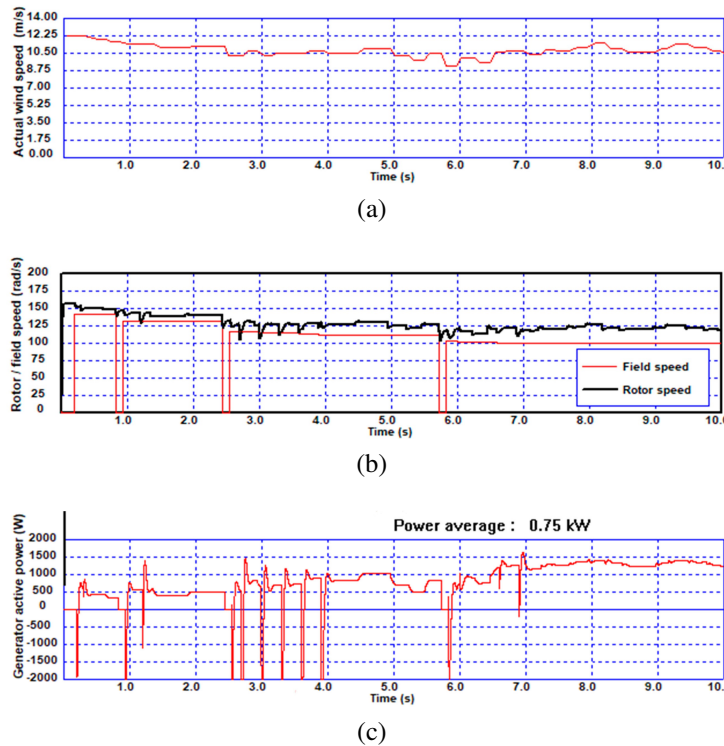


Figure 9. MPPT test results on the SEIG-WTS with a actual wind speed profile for 10 seconds; (a) actual wind speed profile, (b) rotor and magnetic field speed, and (c) generator active power

Finally, the MPPT algorithm was tested with actual wind speed profile for 50 seconds shown in Figure 10(a), which varies between 6.5 to 12.25 m/s. In Figure 10(b) the angular magnetic field speed generated by the MPPT algorithm and the angular rotor speed are shown and in Figure 10(c) the generated active power is shown with an average of 0.82 kW. The optimization proposals of the SEIG-wind turbine system optimize the wind turbine power, which as shown in Figure 3, for each wind speed, the maximum power point of the wind turbine corresponds to an angular rotor speed. Basically, the angular rotor speed that corresponds to the maximum power point of the wind turbine is determined and the SEIG is controlled so that the rotor operates at this speed. Since complex sensors are required to measure the wind turbine power, some proposals develop torque observers [14], performing the indirect power calculation [16]. In this work, the proposal optimizes the SEIG active power that is calculated with the stator voltages (are calculated for the MPPT algorithm) and stator currents that are measured with simple hall effect sensors and the angular magnetic field speed of the SEIG is perturbed.

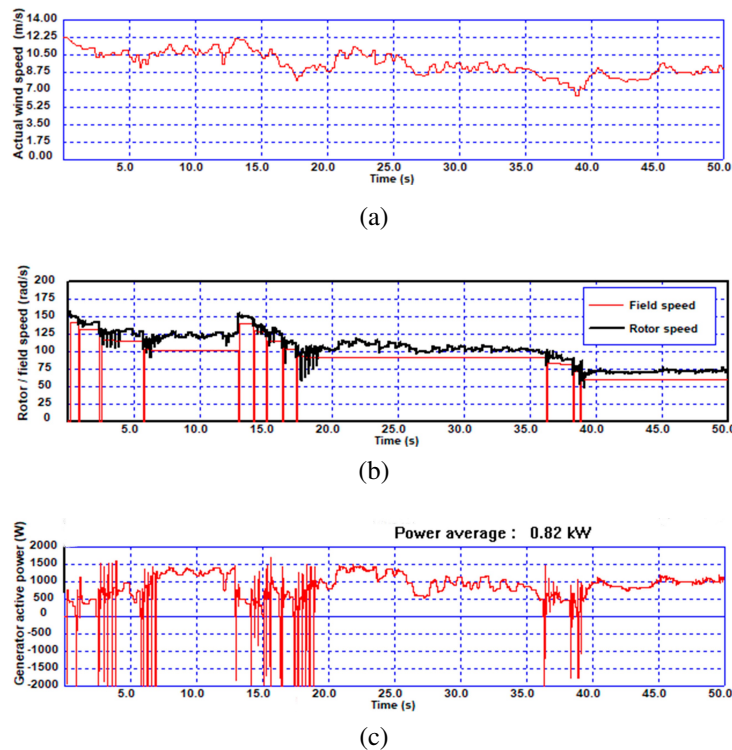


Figure 10. MPPT test results on the SEIG-WTS with a actual wind speed profile for 50 seconds; (a) actual wind speed profile, (b) rotor and magnetic field speed, and (c) generator active power

On the other hand, the rotor angular speed required for the generator to operate at the maximum power point is not calculated since the perturbation of the angular magnetic field speed, indirectly controls the angular rotor speed of the system. The SEIG generates more electric energy when it operates at the rated rotor speed and is reduced when it operates at high or low rotor speeds [31], which is confirmed in the power curve of the Figure 9(c), where up to 2.5 seconds operates at an approximate rotor speed of 140 rad/s and the average active power generated is 500 W, up to 5.8 seconds operates at an approximate rotor speed of 128 rad/s with an average active power generated of 800 W and then it operates at a rotor speed close to 110 rad/s with an active power generated greater than 1000 W, this is because the rated rotor speed of the SEIG is 100 rad/s.

To avoid the abrupt change in angular rotor speed when searching for the maximum power point, the proposed MPPT algorithm releases the rotor. For this, reference voltage is not applied to the stator. Due to the effect of the wind, the angular rotor speed rises and reaches the steady state value as shown in Figure 9(b) at time 2.5 seconds. Then the search for the maximum power point begins by applying the reference voltage to the stator with the frequency that generates a magnetic field with an angular speed slightly less than the angular rotor speed. and is reduced every 0.3 seconds by  $\Delta\omega_0$  until reaching the point of maximum power.

This is because if the magnetic field speed begins to reduce starting from the rotor speed, the power rises until it reaches a maximum value and then reduces [31].

#### 4. CONCLUSION

This paper has proposed a MPPT algorithm based on the P&O approach, applied to the SEIG-WTS. In this MPPT algorithm the angular magnetic field speed of the SEIG is used as the perturbed variable and the active power generated by the SEIG as the observed variable. The performance of the suggested MPPT algorithm has been tested through simulation results analysis which has good results of the maximum active power point tracking with actual wind speed profile. Moreover, the proposed MPPT algorithm has a simple practical implementation because the instantaneous stator currents are measured for the calculation of the observed active power and the angular rotor speed are measured for the calculation of the value of the angular magnetic field speed to start the tracking of the maximum power point. The future challenge will be then to develop a hybrid MPPT algorithm to reduce the maximum tracking time of the maximum power point, which in this proposal is 7 seconds.

#### REFERENCES

- [1] B. A. Nasir, "An accurate dynamical model of induction generator utilized in wind energy systems," *Indonesian Journal of Electrical Engineering and Computer Science (IJECS)*, vol. 27, no. 3, pp. 1185-1198, 2022, doi: 10.11591/ijecs.v27.i3.pp1185-1198.
- [2] H. H. Kadhum, A. S. Alkhafaji, and H. H. Emawi, "The influence of iron losses on selecting the minimum excitation capacitance for self-excited induction generator (SEIG) with wind turbine," *Indonesian Journal of Electrical Engineering and Computer Science (IJECS)*, vol. 19, no. 1, pp. 11-22, 2020, doi: 10.11591/ijecs.v19.i1.pp11-22.
- [3] R. Nazir, S. Syafii, A. Pawawoi, F. Akbar, and Y. Arfan, "Effect analysis of residual magnetism availability level on the success of voltage generation processes in self-excited induction generators," *International Journal of Power Electronics and Drive Systems (IJPEDS)*, vol. 11, no. 3, pp. 1211-1219, 2020, doi: 10.11591/ijpeds.v11.i3.pp1211-1219.
- [4] A. J. Ali, M.Y. Suliman, L. A. Khalaf, and N. S. Sultan, "Performance investigation of stand-alone induction generator based on STATCOM for wind power application," *International Journal of Electrical and Computer Engineering (IJECE)*, vol. 10, no. 6, pp. 5570-5578, 2020, doi: 10.11591/ijece.v10i6.pp5570-5578.
- [5] M. Mokhtari, S. Zouggar, N. K. M'Sirdi, and M. L. Elhafyani, "Voltage regulation of an asynchronous wind turbine using STATCOM and a control strategy based on a combination of single input fuzzy logic regulator and sliding mode controllers," *International Journal of Power Electronics and Drive Systems (IJPEDS)*, vol. 11, no. 3, pp. 1557-1569, 2020, doi: 10.11591/ijpeds.v11.i3.pp1557-1569.
- [6] R. Leidhold, G. Garcia, and M. I. Valla, "Field-oriented controlled induction generator with loss minimization," *IEEE Transactions on Industrial Electronics*, vol. 49, no. 1, pp. 147-156, 2002, doi: 10.1109/41.982258.
- [7] D. Seyoum, M. F. Rahman, and C. Grantham, "Terminal voltage control of a wind turbine driven isolated induction generator using stator oriented field control," *Eighteenth Annual IEEE Applied Power Electronics Conference and Exposition*, vol. 2, pp. 846-852, 2003, doi: 10.1109/APEC.2003.1179315.
- [8] T. Ahmed, O. Noro, E. Hiraki, and M. Nakaoaka, "Terminal voltage regulation characteristics by static var compensator for a three-phase self-excited induction generator," *IEEE Transactions on Industry Applications*, vol. 4, no. 4, pp. 978-988, 2004, doi: 10.1109/TIA.2004.830783.
- [9] G. Kenne, C. T. Sanjong, and E. M. Nfah, "Adaptive PI Control Strategy for a Self-Excited Induction Generator Driven by a Variable Speed Wind Turbine," *Journal of Circuits, Systems and Computers*, vol. 26, no. 2, 2017, doi: 10.1142/S0218126617500244.
- [10] S. Peresada, S. Kovbasa, S. Korol, N. Pechenik, and N. Zhelinskyi, "Indirect field oriented output feedback linearized control of induction generator," *IEPS*, pp. 1-5, 2016, doi: 10.1109/IEPS.2016.7521881.
- [11] S. Bozhko, S. Peresada, S. Kovbasa, and M. Zhelinskyi, "Robust indirect field oriented control of induction generator," *ESARS-ITEC*, pp. 1-6, 2016, doi: 10.1109/ESARS-ITEC.2016.7841421.
- [12] H. H. Mousa, A.-R. Youssef, and E. E. M. Mohamed, "State of the art perturb and observe MPPT algorithms based wind energy conversion systems: A technology review," *International Journal of Electrical Power & Energy Systems*, vol. 126, no. A, 2021, doi: 10.1016/j.ijepes.2020.106598.
- [13] J. Mishra, M. Pattnaik, and S. Samanta, "Load Voltage based MPPT Algorithm for a Stand-alone Wind Generation System," *INDICON 2018*, pp. 1-4, 2018, doi: 10.1109/INDICON45594.2018.8986998.
- [14] M. Bašić, M. Bubalo, D. Vukadinović, and I. Grgić, "Sensorless Maximum Power Control of a Stand-Alone Squirrel-Cage Induction Generator Driven by a Variable-Speed Wind Turbine," *Journal of Electrical Engineering & Technology*, vol. 16, pp. 333-347, 2021, doi: 10.1007/s42835-020-00582-8.
- [15] S. Arika, A. Hemant, B. Vikas, and S. Sachin, "Control Implementation of Squirrel Cage Induction Generator based Wind Energy Conversion System," *Journal of Scientific & Industrial Research*, vol. 9, no. 4, pp. 306-311, 2020, doi: 10.56042/jsir.v79i4.68675.
- [16] S. A. Khadate, B. S. V. Sai, and D. Chatterjee, "A Model Based Control Strategy for Variable Speed Operation of Three Phase Induction Generator," *CISPSSSE*, pp. 1-5, 2020, doi: 10.1109/CISPSSSE49931.2020.9212283.
- [17] M. Rahimi, M. Asadi, "Control and dynamic response analysis of full converter wind turbines with squirrel cage induction generators considering pitch control and drive train dynamics," *International Journal of Electrical Power & Energy Systems*, vol. 108, pp. 280-292, 2019, doi: 10.1016/j.ijepes.2019.01.018.
- [18] C. Lavanya and K. Sujesh, "MPPT Control Technique for Stand-Alone Wind Energy Conversion System," *IJETR*, vol. 7, no. 7, pp. 1312-1315, 2018.
- [19] T. Amieur, D. Taibi, and O. Amieur, "Voltage oriented control of self-excited induction generator for wind energy system with

- MPPT," in *AIP Conference Proceedings*, 2018, vol. 1968, doi: 10.1016/j.ijepes.2019.01.018.
- [20] J. Mishra, M. Pattnaik, and S. Samanta, "Drift-Free Perturb and Observe MPPT Algorithm With Improved Performance for SEIG-Based Stand-Alone Wind Energy Generation System," *IEEE Transactions on Power Electronics*, vol. 35, no. 6, pp. 5842-5849, 2020, doi: 10.1109/TPEL.2019.2952324.
- [21] H. Laghridat, A. Essadki, M. Annoukoubi, and T. Nasser, "Comparative Analysis between PI and ADRC Control of a Variable Speed Wind Energy Conversion System using a Squirrel Cage Induction Generator," *IRSEC*, vol. 1, pp. 1-6, 2020, doi: 10.1109/IR-SEC.2018.8702989.
- [22] M. Zribi, M. Alrifai, and M. Rayan, "Sliding Mode Control of a Variable-Speed Wind Energy Conversion System Using a Squirrel Cage Induction Generator," *Energies*, vol. 10, no. 5, p. 604, 2017, doi: 10.3390/en10050604.
- [23] H. Zhao and Q. Wu, *Adaptive Control of Wind Turbines for Maximum Power Point Tracking*, Chapter 7, Modeling and Modern Control of Wind Power, 2017, doi: 10.1002/9781119236382.ch7.
- [24] M. A. Zeddini, R. Pusca, A. Sakly, and M. F. Mimouni, "PSO-based MPPT control of wind-driven Self-Excited Induction Generator for pumping system," *Renewable Energy*, 2016, vol. 95, pp. 162-177, doi: 10.1016/j.renene.2016.04.008.
- [25] A. E. Yaakoubi, A. Asselman, A. Djebli, and E. H. Aroudam, "A MPPT Strategy Based on Fuzzy Control for a Wind Energy Conversion System," *Procedia Technology*, 2016, vol. 22, pp. 697-704, doi: 10.1016/j.protcy.2016.01.145.
- [26] T. A. Brasil, L. F. Crispino, and W. Suemitsu, "Fuzzy MPPT control of grid-connected three-phase induction machine for wind power generation," *ISIE*, 2015, pp. 803-807, doi: 10.1109/ISIE.2015.7281572.
- [27] B. Dumnic, B. Popadic, D. Milicevic, V. Katic, and D. Oros, "Speed-sensorless vector control of a wind turbine induction generator using artificial neural network," *EPEPEMC*, 2014, pp. 371-376, doi: 10.1109/EPEPEMC.2014.6980521.
- [28] X. Liu, J. Liu, S. Laghrouche, M. Cirrincione, and M. Wack, "MPPT control of variable speed wind generators with squirrel cage induction machines," *EFEA*, 2014, pp. 1-6, doi: 10.1109/EFEA.2014.7059935.
- [29] M. G. B. Borja, S. Lescano, and J. E. Luyo, "Dynamic behavior of the wind turbine - self-exciting induction generator system, using a reference voltage of variable frequency as excitation," *2021 IEEE CHILEAN Conference on Electrical, Electronics Engineering, Information and Communication Technologies (CHILECON)*, 2021, pp. 1-6, doi: 10.1109/CHILECON54041.2021.9703069.
- [30] H. Habibi, H. R. Nohooji, and I. Howard, "Power maximization of variable-speed variable-pitch wind turbines using passive adaptive neural fault tolerant control," *Frontiers of Mechanical Engineering*, vol. 95, pp. 162-177, 2016, doi: 10.1007/s11465-017-0431-4.
- [31] M. G. B. Borja, S. Lescano, and J. E. Luyo, "Dynamic behavior analysis of the three-phase self-excited induction generator during electricity generation with variable energy sources," *CHILECON 2019*, 2019, pp. 1-6, doi: 10.1109/CHILECON47746.2019.8987637.

## BIOGRAPHIES OF AUTHORS



**Mario G. Borja Borja** received the Master of Science degree in Industrial control, Industrial Complex Automation and Robotics systems from National Technical University of Ukraine, Ukraine, in 1996. He received the Ph.D. degree in Energetic from National University of Engineering, Lima, in 2023. Currently he is Research Professor of System Control, Automatic and Robotic Industrial Research Laboratory, Department of Mechanical Engineering, National University of Engineering, Lima. His research interests include control strategies for AC machine drives and renewable energy. He can be contacted at email: mborjab@uni.edu.pe.



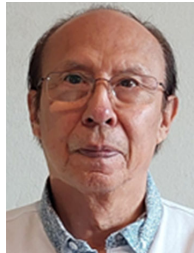
**Sergio Lescano** is the founder and CEO of Amarob Technologies. Before specializing in entrepreneurship at HEC-Paris (Challenge+program), he realized his Ph.D. thesis at FEMTO-ST (CNRS 6174 - UBFC) as part of the European FP7 project RALP, where he worked on the design, fabrication and control of the microrobot placed in the laryngoscope distal-end, destined to guide a laser beam onto the vocal fold. He is co-inventor of three patents (2 on the microrobot, 1 on a haptic stylus). He has participated to several collaborative projects (FP7 RALP, ANR GreenShield, and BPI FrenchTech). He can be contacted at email: sergio.lescano@amarob.com.



**Sally Torres Alvarado** received the Master of Science degree in Computer and Network Systems from National Technical University of Ukraine, Ukraine, in 1996. She received the Ph.D. degree in Systems from National University Federico Villareal, Lima, in 2020. Currently she is Research Professor of Dynamic of Systems and Natural Language Processing Research Laboratory, Department of Systems, Engineering National University of Callao, Lima. Her research interests include dynamic behaviour of systems and natural language processing of Spanish. She can be contacted at email: sktorresa@unac.edu.pe.



**Ubaldo Yancachajlla Tito** received the Engineer degree in Mechanical Engineering from National Aviation University (NAU) of Ukraine in 1997. He received the Master degree in Machine Design from National Engineering University, Peru in 2010 and completed his Doctoris Scientiae in Science, Technology and Environment from the National University of the Altiplano, Peru, in 2022. Currently he is Research Professor of wind energy engineering-Department of Renewable Energy Engineering, Faculty of Engineering Sciences- National University of Juliaca, Peru. His research interests include hybrid power systems, renewable energy, solar power, solar radiation, wind power, and wind power plants. He can be contacted at email: uyancachajlla@unaj.edu.pe.



**Jaime E. Luyo** Graduated, Unanimous Distinction, at the National University of Engineering, UNI, Lima, Peru. Master of Science in Electrical Engineering, Rensselaer Polytechnic Institute, U.S.A. Ph.D. in Eco-nomics from the National Major University of San Marcos, UNMSM, Best Student, Lima, Peru. He is General Coordinator and professor of the Ph.D. Energetics Program at UNI. Former Dean at UNMSM. Books: "The Energy in the XXI Century. Contributions to Peruvian sustainable energy development" (co-author, 2023); "The Real Electric Market and its Faults. Foundations and experiences in Peru and Latin America" (2016); "The Energy Sector in Peru: Reforms, Crisis, Regulation and Regional Integration" (2012). Research fields and expertise in: planning and energy policy and electric power systems economics. He can be contacted at email: jluyok@uni.edu.pe.